

multiSMD - Case Studies

Katarzyna Walczewska-Szewc ^{1*}, Beata Niklas ², Wiesław Nowak ¹

1. Institute of Physics, Faculty of Physics, Astronomy and Informatics, Nicolaus Copernicus University in Toruń, ul. Grudziądzka 5, 87-100 Toruń, Poland;

2. Department of Animal Physiology and Neurobiology, Faculty of Biological and Veterinary Sciences, Nicolaus Copernicus University, Lwowska 1, 87-100, Toruń, Poland

* kszewc@umk.pl

Case study I: SARS-CoV-2 spike protein-ACE2 complex anisotropy in mechanical stability

We applied our method to the SARS-CoV-2 spike protein-ACE2 complex to examine anisotropy in mechanical stability, addressing the key question: What forces are required to disrupt this protein-protein interaction in multiple directions?

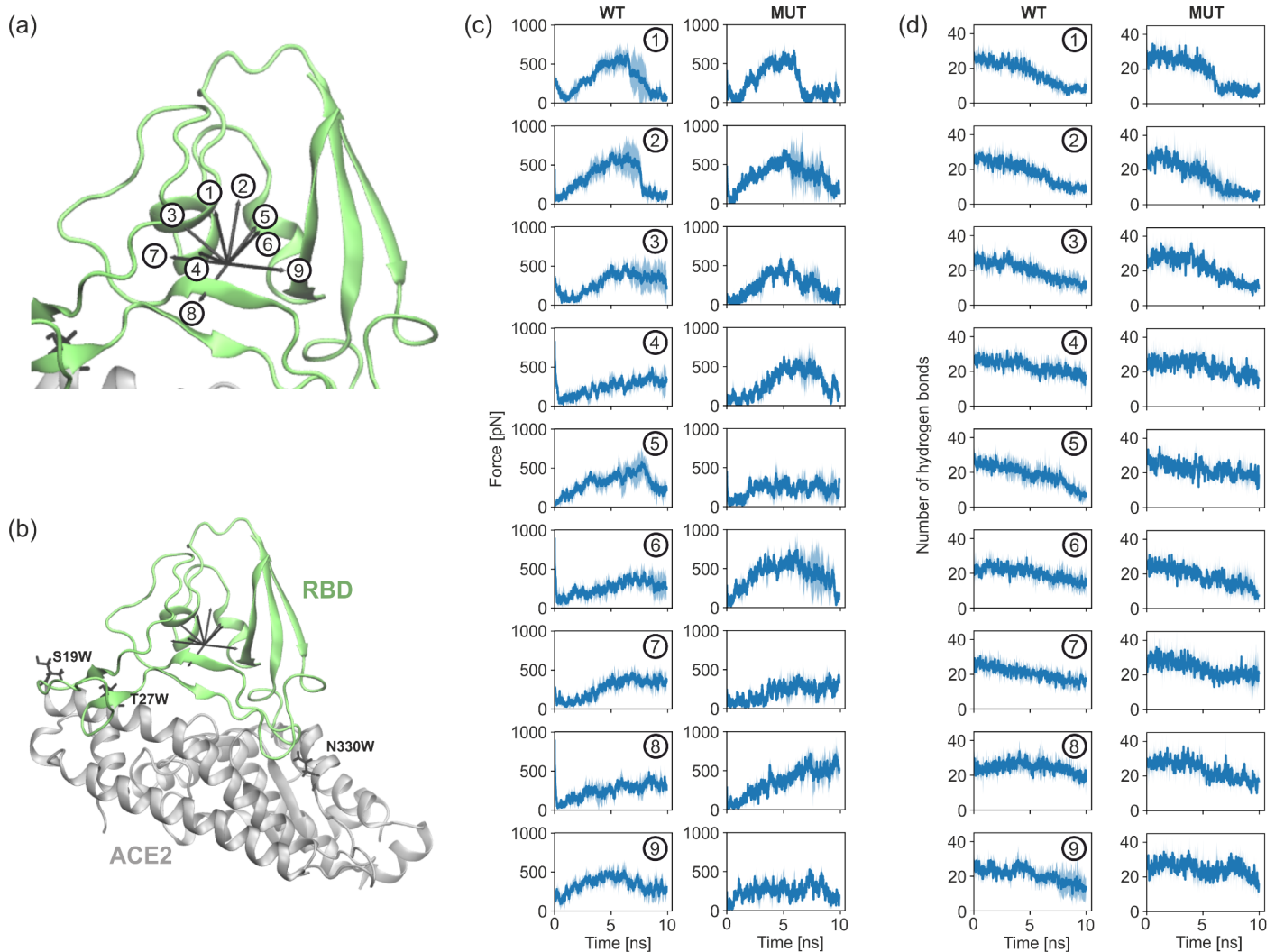


Figure 2: Multi-directional analysis of SARS-CoV-2 S - ACE2 unbinding. (a) Schematic of nine pulling directions applied to the complex. (b) Simulation system of truncated S - ACE2 complex shown in green and gray with mutated residues shown as black sticks. (c) Maximum disruption forces across pulling directions for wild-type (WT) versus mutant (MUT) complexes. (d) Hydrogen bond dynamics during S-protein pulling.

We first evaluated the efficacy of our multiSMD program by applying it to the COVID-19 relevant protein system. A key stage of viral infection is the interaction between viral spike proteins and human angiotensin-converting enzyme 2 (ACE2) receptor.¹ Current drug discovery strategies for COVID-19 focus on weakening these specific protein-protein interactions by blocking the ACE2 receptor or the viral Spike protein to prevent infection. We thus proceed to measure the forces required to disrupt this complex considering their anisotropy (see Figure 2a for specific directions).

We used the structure of the receptor-binding domain (RBD) of the spike protein bound to ACE2² (PDB ID 6M0J, see Supplementary Figure S2). Using microsecond long MD simulation of the complex³ we were able to extract a structurally stable fragment of the complex interface (see Supplementary information for details). We also performed *in silico* mutagenesis of the ACE2 receptor, focusing on three mutations, S19W, T27W, and N330Y (see Figure 2b), previously shown to enhance SARS-CoV-2 S-RBD binding⁴, to investigate their impact on SMD pulling forces. The structures of the SARS-CoV-2 S-RBD bound to the ACE2 mutants reveal that the increased binding affinity is mainly due to van der Waals interactions created by the aromatic side chains of W19, W27, and Y330.

After equilibration and 0.25 μ s of classical MD simulation using NAMD performed to stabilize the system, we run our multiSMD.py script to generate inputs for SMD simulations in nine directions of pulling (see Figure 2a). We run 5 replicas of 10 ns SMD in each direction for non-modified complex (APO) and mutated system (MUT).A detailed description of the methods and investigated system is provided in the Supplementary Information.

We based our analysis on a calculation of (i) the changing number of hydrogen bonds when pulling the RBD in various directions (Figure 2d), and (ii) forces required to disrupt the complex (Figure 2c). In a simulation time as short as 10 ns, we observed a significant anisotropy in the complex's response to external forces. In a system without modifications (WT), pulling in all directions resulted in the reduction in the number of hydrogen bonds. However, when mutations were introduced, the number of hydrogen bonds was constant upon pulling in some directions (see WT 4, 5, and 7 in Figure 2d). Greater forces were also required to disrupt the mutated complex, although not in all directions tested. These results suggest stronger interactions between RBD and ACE2 when substitutions to residues with aromatic side chains are present, which may enhance virulence. One should bear in mind that the simulations were performed using only interacting parts of both proteins (not a full system) so the allosteric effects were not possible to capture and only part of protein S – ACE2 interactions were analyzed.

Case study II: The comparison of ATP unbinding from potassium ion channels fragments Kir6.1 and Kir6.2.

Inward-rectifying potassium (Kir6.x) proteins (Figure 3a) are the pore-forming subunits of ATP-sensitive potassium channels (KATP). These channels regulate the flow of potassium ions, and thus the membrane excitability, based on the energy level of the cell (the ratio of ATP to ADP)⁵. Different combinations of Kir6.1 and Kir6.2 and sulfonylurea receptor (SUR1, SUR2a, and SUR2b) subunits generate various KATP subtypes with distinct tissue distributions and functions⁶. Despite significant sequence and structural similarity, Kir6.1 and Kir6.2 isoforms differ in their sensitivity to ATP^{7,8}. The ATP-binding site in both isoforms is highly conserved, with nearly identical residues involved in ligand interaction, as confirmed by available cryo-EM structures (eg. 6C3P⁹ and 7MIT⁷) and our unbiased MD simulations. MD snapshots illustrating ATP bound to Kir6.1 and Kir6.2 are shown in Figure 3c,e. Figure S4 illustrates the frequency of close contacts between individual residues and ATP throughout three unbiased short simulations.

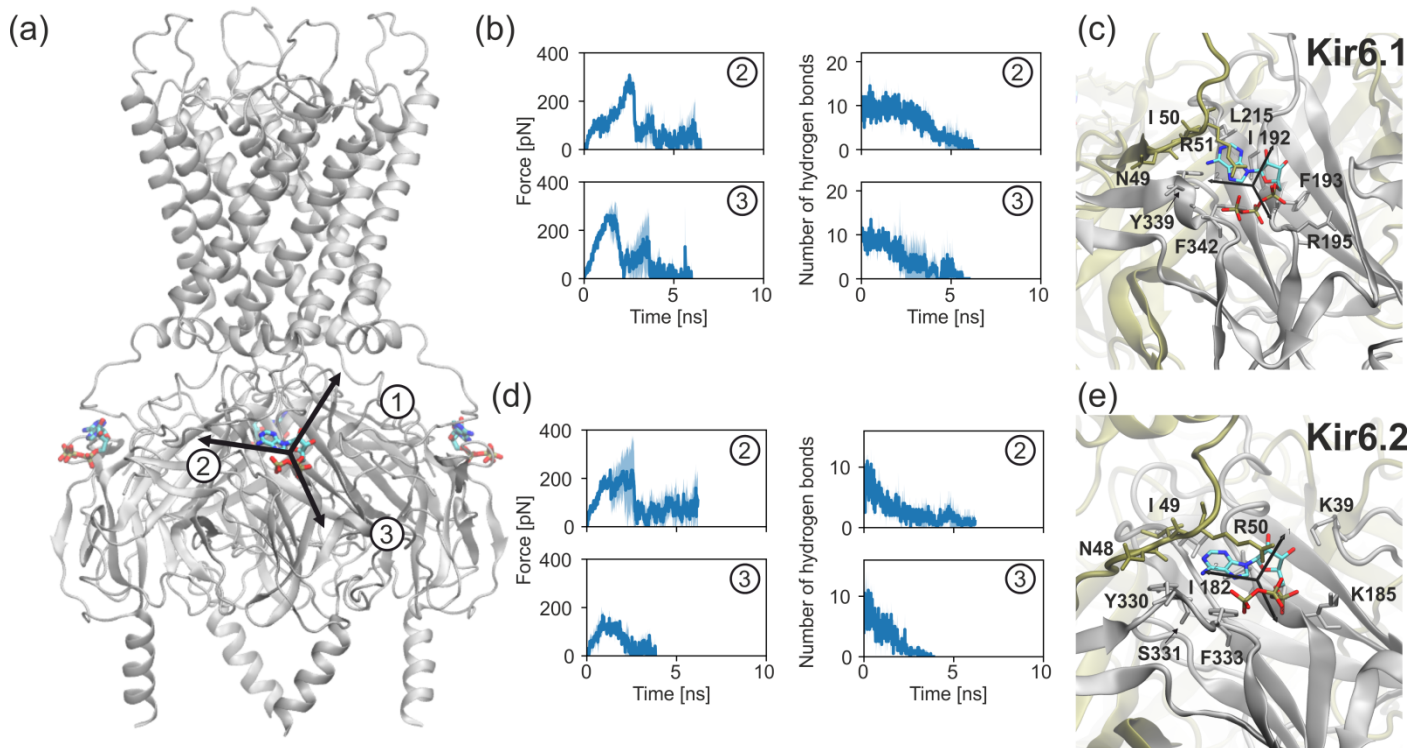


Figure 3. Direction-dependent ATP unbinding from Kir6.1/Kir6.2 channels. (a) Structural overview of Kir6.x tetramer (cartoon) with bound ATP (sticks). (b,d) Force profiles during ATP extraction along direction 2 and direction 3, showing Kir6.1 (b) versus Kir6.2 (d). (c,e) MD snapshots of ATP (cyan) binding sites in Kir6.1 (c) and Kir6.2 (e), highlighting key residues (sticks).

Experimental studies have reported notable differences in ATP-binding between the isoforms despite the high conservation of the ATP-binding site^{7,8}. One distinguishing feature is the substitution of R195 in Kir6.1 with K185 in Kir6.2. Both residues are positively charged and critical for ATP binding, yet the substitution may subtly influence ligand interaction. To explore this further, we applied our multiSMD method to evaluate the forces required to extract ATP from the binding pocket at a constant velocity of 0.0005 nm/ps. Starting from equilibrated Kir6.1 and Kir6.2 systems, we pulled ATP along three directions, recording unbinding forces until complete ligand dissociation (three repeats for each pulling direction).

We excluded the first pulling direction from analysis, as the ATP trajectory led to the cell membrane, which has no physiological rationale. Our results show significant differences in forces required for pulling along the third direction, where Kir6.1 requires 1.5 times greater force than Kir6.2. In turn, pulling along the second direction yields similar force profiles for both isoforms (Figure 3b,d). Notably, direction 3 leads ATP toward the region involving the R195/K185 substitution. Analysis suggests that R195 in Kir6.1 forms stronger electrostatic interactions with the triphosphate moiety of ATP than K185 in Kir6.2, which may explain the observed difference. For the third pulling direction, forces required to pull the ATP molecule out of its binding site were higher for Kir6.1 than for Kir6.2, and a greater amount of time was required to break the hydrogen bonds between the Kir6.1 protein and the ligand.

These findings are consistent with the hypothesis that Kir6.1 may exhibit tighter ATP binding compared to Kir6.2, at least in the context of the isolated Kir6 tetramer. However, it is important to note that ATP sensitivity in the full KATP channel complex (including the SUR subunit) is influenced by additional factors, such as interactions with SUR, the presence of Mg-nucleotides, and interactions with PIP2, which are not captured in our simplified model. For instance, Kir6.1-containing channels require Mg-nucleotides to open and exhibit lower open probability compared to Kir6.2-containing channels, despite potentially stronger ATP binding to Kir6.1^{7,8,10}. Thus, while our simulations provide insights into the local differences in ATP-binding mechanics between Kir6.1 and Kir6.2, they do not fully explain the physiological differences in ATP sensitivity observed in the complete KATP channel complex.

These preliminary findings highlight the potential of our multidirectional SMD method for identifying subtle yet functionally significant differences in ligand binding and interaction sites. Further energetic analysis, for example with metadynamics, as well as simulations incorporating the full KATP channel complex, will be needed to confirm these results and provide deeper insights into the interplay between ATP binding, channel gating, and regulation by SUR subunits

Case study III: KNt Release from SUR2B Pocket in Vascular KATP Channels.

The tight interaction between Kir6.x and SUR subunits, which involves both their interfacial contacts and the interactions of disordered regions, is a recently described feature of KATP channels^{7,11–14}. In vascular KATP channels (Kir6.1/SUR2B), the N-terminus of Kir6.1 (KNt) strengthens this interaction by docking into a distal pocket of SUR2B. A similar mechanism occurs in pancreatic KATP channels (Kir6.2/SUR1), suggesting a conserved regulatory role. This interaction, through a not yet fully understood mechanism, leads to channel closure. In cryo-EM structures of closed KATP channels, electron densities corresponding to the N-terminus of Kir6 can be observed within this pocket^{7,14}. However, the N-terminus is absent from the pocket in open-channel structures where SUR NBD domains are dimerized, suggesting a physiological insertion and removal process¹⁵. This indicates that KNt should effortlessly exit the pocket when required.

The process of KNt release from the SUR2B pocket is enigmatic. Its directionality is unclear because KNt, an intrinsically disordered region (IDR), lacks a defined position outside the pocket. This makes it an ideal system for testing our multiSMD approach. A simulation system comprises SUR2B with the KNt region of Kir6.1 inserted into the pocket (Figure 4a), representing a fragment of the vascular KATP channel. We started with unbiased MD simulations to equilibrate the system. Two systems were constructed: one without ligands and another with glibenclamide in the pocket. Glibenclamide stabilizes the KNt position and supports the inward-open conformation of SUR2B, corresponding to the KATP channel's closed state¹⁴.

The frequency of close contacts between KNt and SUR residues in the unbiased simulation is presented as bar plots in Figures 4b and 4c (for systems without a ligand and with glibenclamide, respectively). Snapshots illustrating the position of KNt within the pocket and surrounding residues are also shown. We identified two possible pulling directions for KNt for the SMD simulations, denoted as directions 1st and 2nd (Figure 4a). Artificial pulling forces were applied to the proximal part of KNt (residues 20-22), allowing us to evaluate which direction requires less force and, consequently, suggests a more straightforward release pathway.

The profiles of forces required to extract the distal KNt region (residues 1-10) from the pocket in a function of simulation time, are shown in blue plots in Figures 4b and 4c for systems without and with glibenclamide, respectively. The graphs cut off at the point where KNt fully exits the SUR1 pocket. Significant differences between the first and the second pulling directions were observed. For the first direction, a force of approximately 400 pN was initially required to overcome strong interactions between SUR's E1196 and KNt's K24 as well as E1173 and R23. These residues form stable interactions that must be disrupted for the KNt tail to exit the pocket. In this case, the force is applied tangentially to the expected direction of those interactions, which is less effective than applying it perpendicularly. Therefore, pulling along the second direction was initially easier, with resistance increasing as the distal KNt region began leaving the pocket.

Notably, the presence of glibenclamide slightly increased the force required for KNt extraction, particularly in the second direction. While these findings suggest potential pathways and interactions affecting KNt release, more precise methods, such as umbrella sampling or metadynamics, are necessary for a detailed potential of mean force characterization of the process.

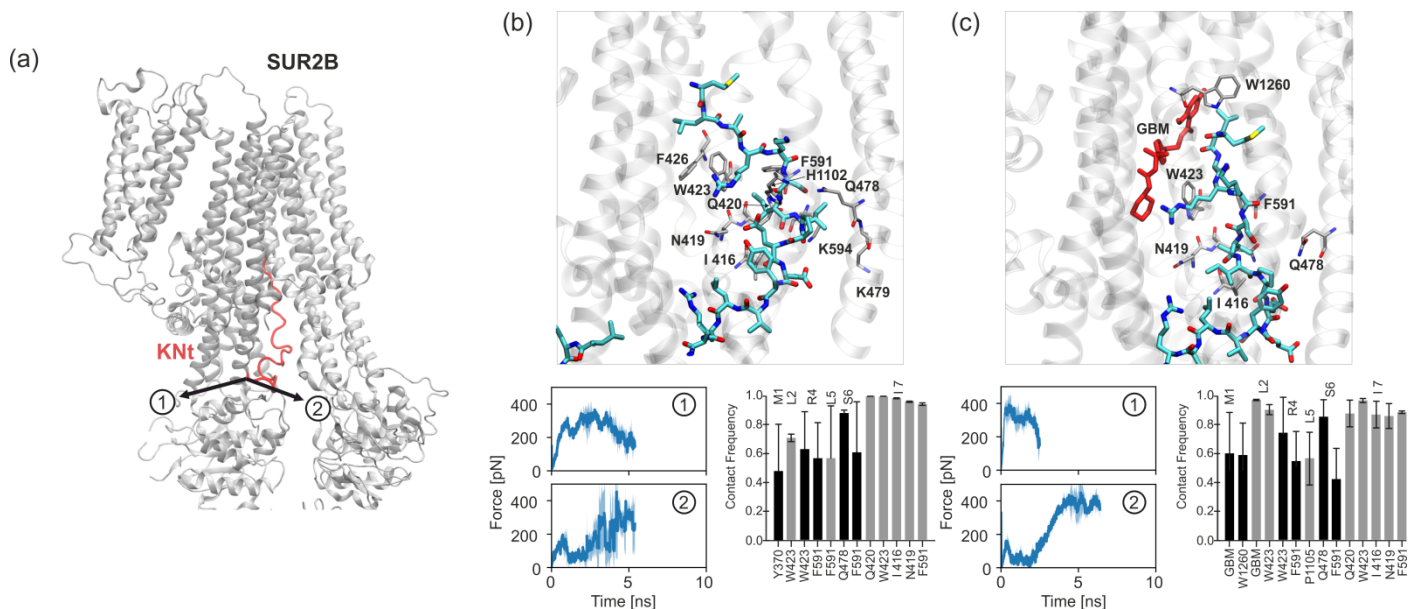


Figure 4: Multi-directional analysis of KNt release from SUR2B. (a) System overview with two tested pulling directions (arrows). (b) System without a ligand: a snapshot of binding pocket (upper, KNt shown as cyan sticks, SUR2B residues are shown as gray sticks), extraction force profiles (lower left), and KNt-SUR2B contact frequencies (lower right). (c) System with glibenclamide: a snapshot of binding pocket (upper, GBM shown in red), extraction force profiles (lower left), and KNt-SUR2B contact frequencies (lower right).

References:

1. Zhou, P. *et al.* A pneumonia outbreak associated with a new coronavirus of probable bat origin. *Nature* **579**, 270–273 (2020).
2. Lan, J. *et al.* Structure of the SARS-CoV-2 spike receptor-binding domain bound to the ACE2 receptor. *Nature* **581**, 215–220 (2020).
3. Spinello, A., Saltalamacchia, A. & Magistrato, A. Is the Rigidity of SARS-CoV-2 Spike Receptor-Binding Motif the Hallmark for Its Enhanced Infectivity? Insights from All-Atom Simulations. *J Phys Chem Lett* **11**, 4785–4790 (2020).
4. Ye, F. *et al.* S19W, T27W, and N330Y mutations in ACE2 enhance SARS-CoV-2 S-RBD binding toward both wild-type and antibody-resistant viruses and its molecular basis. *Signal Transduct Target Ther* **6**, 343 (2021).
5. Driggers, C. M. & Shyng, S.-L. Mechanistic insights on KATP channel regulation from cryo-EM structures. *J Gen Physiol* **155**, (2023).
6. Patton, B. L., Zhu, P., ElSheikh, A., Driggers, C. M. & Shyng, S.-L. Dynamic duo: Kir6 and SUR in K channel structure and function. *Channels (Austin)* **18**, 2327708 (2024).

7. Sung, M. W. *et al.* Vascular K channel structural dynamics reveal regulatory mechanism by Mg-nucleotides. *Proc Natl Acad Sci U S A* **118**, (2021).
8. Quinn, K. V., Cui, Y., Giblin, J. P., Clapp, L. H. & Tinker, A. Do anionic phospholipids serve as cofactors or second messengers for the regulation of activity of cloned ATP-sensitive K⁺ channels? *Circ Res* **93**, 646–655 (2003).
9. Lee, K. P. K., Chen, J. & MacKinnon, R. Molecular structure of human KATP in complex with ATP and ADP. *Elife* **6**, (2017).
10. Vanoye, C. G. *et al.* The carboxyl termini of K(ATP) channels bind nucleotides. *J Biol Chem* **277**, 23260–23270 (2002).
11. Wu, J.-X. *et al.* Ligand binding and conformational changes of SUR1 subunit in pancreatic ATP-sensitive potassium channels. *Protein Cell* **9**, 553–567 (2018).
12. Martin, G. M. *et al.* Mechanism of pharmacochaperoning in a mammalian K channel revealed by cryo-EM. *Elife* **8**, (2019).
13. Walczewska-Szewc, K. & Nowak, W. Structural Determinants of Insulin Release: Disordered N-Terminal Tail of Kir6.2 Affects Potassium Channel Dynamics through Interactions with Sulfonylurea Binding Region in a SUR1 Partner. *J Phys Chem B* **124**, 6198–6211 (2020).
14. Sung, M. W. *et al.* Ligand-mediated Structural Dynamics of a Mammalian Pancreatic K Channel. *J Mol Biol* **434**, 167789 (2022).
15. Driggers, C. M., Kuo, Y.-Y., Zhu, P., ElSheikh, A. & Shyng, S.-L. Structure of an open K channel reveals tandem PIP binding sites mediating the Kir6.2 and SUR1 regulatory interface. *Nat Commun* **15**, 2502 (2024).